Towards full-body X-ray images

Christoph Luckner[1,2], Thomas Mertelmeier[2], Andreas Maier[1], Ludwig Ritschl[2]

[1]Pattern Recognition Lab, FAU Erlangen-Nuernberg
[2]Siemens Healthcare GmbH, Forchheim
christoph.luckner@fau.de

Abstract. Digital tomosynthesis is a tomographic imaging technique whose upsurge is mainly caused by breast imaging. However, it might also be useful in orthopedics due to its high in-plane resolution as well as the fact that tomosynthetic slices do not suffer from magnification or distortion, making measurements possible, for example, even without the need of any calibration object. Since the reading time of such a reconstruction is higher compared to conventional 2-D radiographs, a simple parallel projection of the volume can be computed to get an overview of the volume. However, this leads to a rather blurred image impression since all artifacts and inhomogeneities in the reconstructed volume as well as certain anatomical structures which are not necessary for the diagnosis, will end up in the projection. We propose a method which selects the slices to be projected into a smart synthetic X-ray image in a way which is optimal w.r.t to the sharpness of predefined ROIs (e. g. knee, spine or hip). Therefore, two Laplacian-based auto-focus measures are combined with a thin-plate spline yielding a sharp and homogenous image impression within the smart radiograph. It was shown that the auto-focus method is able to select the same slice as have been selected during an expert annotation. Upon visual inspection, it could be determined that the proposed method achieves higher contrast and clearly better visibility of complex bone structures like spine or hip.
The concepts and information presented in this paper are based on research and are not commercially available.

1 Introduction

Digital tomosynthesis (DT) is a tomographic imaging technique using flat panel detectors, which allows creating multiple tomographic images in a specified plane. Its upsurge is mainly caused by breast imaging, however, it might also be useful in orthopedics. Even though DT is characterized by an incomplete data acquisition, meaning that it fails to provide a complete and isotropic 3-D imaging of the scanned object, especially its high in-plane resolution as well as the fact that reconstructed slices do not suffer from magnification or distortion compensate its drawbacks. The former yields that DT provides excellent visibility of fine structures, necessary for the assessment of high contrast structures like bone and joint structures, which can be difficult to assess in conventional 2-D radiographs. The latter may allow the usage of tomosynthetic datasets for

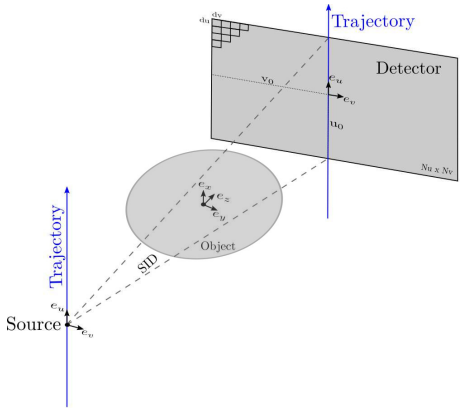

Fig. 1. Acquisition geometry and parallel-shift trajectory (indicated as blue arrows) [3].

surgical planning or the assessment of pathologies since measurements are easily possible even without the need of a dedicated calibration object [1,2]. Since the reading time of a tomosynthetic volume is increased compared to plain 2-D X-rays, a synthetic radiograph can be created based on the 3-D reconstruction by performing a simple parallel projection of all slices. However, this leads to a rather blurred image impression since all artifacts and inhomogeneities in the reconstructed tomo-volume, as well as certain anatomical structures which are not necessary for the diagnosis, will end up in the synthetic radiograph. We, instead, propose a method which selects the slices to be projected into the smart synthetic X-ray image (sSR) in a way which is optimal in terms of sharpness of predefined regions of interest (ROIs).

2 Materials and Methods

In the following, the image acquisition and reconstruction process using filtered backprojection will be outlined. Then, the proposed algorithm to generate sSR using auto-focus measures and thin-plate splines is presented. The results were compared to an average intensity projection and the current state-of-the-art acquisition technique for full-body imaging - the source-tilting technique.

2.1 Image acquisition and reconstruction

The acquisition geometry as well as the parallel-shift line trajectory (indicated as blue arrows) is shown in Fig. 1. The chosen trajectory allows lying as well as standing acquisitions and thus is also capable of weight-bearing acquisitions. The distance between source and detector is denoted as SID. N_u and N_v is the number of pixels in u- and v direction and the corresponding isotropic pixel pitch is denoted as d_u and d_v, respectively. The acquired projections form the basis for the reconstruction, which uses the cone-angle to obtain depth information. To

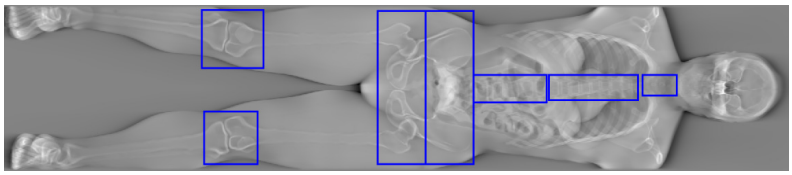

Fig. 2. Central slice of a tomosynthetic reconstruction. The ROIs are outlined in blue.

cope with aliasing artifacts due to the scanning geometry a slice thickness filter as introduced in [3] is used as preprocessing step before the reconstruction, which is performed using the widely-used filtered backprojection. The reconstruction will be denoted as $V(\boldsymbol{x}, z)$, with $\boldsymbol{x} = (x, y)$, consisting of N_x and N_y isotropic pixels in x- and y-direction and N_z slices with slice thickness d_z in z-direction.

2.2 Smart X-ray image generation

The generation of a smart synthetic radiograph consists of four subsequent steps:

1. Define one (or multiple) ROI $\mathcal{R}$ in a tomosynthesis slice. A set of ROIs (knees, hip, lumbar spine, thoracic sp. and cervical sp.) is illustrated in Fig. 2.

$$\mathcal{R}(z) \equiv V(\boldsymbol{x}, z), \text{ with } x, y \in \mathcal{R}$$

2. Compute focus measures α for each ROI $\mathcal{R}$ within each slice.
3. Use best, i. e. sharpest, slice as seed point for a thin-plate spline (TPS).
4. Project the optimal slices (according to the TPS) into the sSR.

Auto-focus measure To determine the degree of focus for a slice z inside an ROI $\mathcal{R}$, we compute two Laplacian-based auto-focus measures α.

The first measure, the Energy of Laplacian (LAPE) [4], is defined as

$$\alpha_{\text{LAPE}}(\mathcal{R}(z)) = \sum_{x,y} \Delta\mathcal{R}(\boldsymbol{x}, z)^2, \tag{1}$$

where $\Delta\mathcal{R}$ is the image Laplacian obtained by a convolution of a slice z of the ROI $\mathcal{R}$ with the Laplacian masks

$$\mathcal{L}_x = [1 \quad -2 \quad 1] \text{ and } \mathcal{L}_y = \mathcal{L}_x^T.$$

The second measure, the diagonal Laplacian (LAPD) [4], is defined as

$$\alpha_{\text{LAPD}}(\mathcal{R}(z)) = |\mathcal{R}(z) * \hat{\mathcal{L}}_x| + |\mathcal{R}(z) * \hat{\mathcal{L}}_y| + |\mathcal{R}(z) * \mathcal{L}_{d1}| + |\mathcal{R}(z) * \mathcal{L}_{d2}|, \tag{2}$$

with $\hat{\mathcal{L}}_x = -\mathcal{L}_x = [-1\ 2\ -1]$ and $\hat{\mathcal{L}}_y = \hat{\mathcal{L}}_x^T$ as modified convolution masks to detect vertical and horizontal structures, and $\mathcal{L}_{d1}$ and $\mathcal{L}_{d2}$ to detect diagonal structures, which are given by

$$\mathcal{L}_{d1} = \frac{1}{\sqrt{2}} \begin{bmatrix} 0 & 0 & 1 \\ 0 & -2 & 0 \\ 1 & 0 & 0 \end{bmatrix} \quad \text{and} \quad \mathcal{L}_{d2} = \frac{1}{\sqrt{2}} \begin{bmatrix} 1 & 0 & 0 \\ 0 & -2 & 0 \\ 0 & 0 & 1 \end{bmatrix}.$$

Since auto-focus measures are prone to noise and artifacts, we apply a moving average filter as a post-processing step to the computed auto-focus measures, to cope with outliers.

Finally, the mean value over the two smoothed auto-focus measures $\widehat{\alpha}$ is computed to obtain a combined and slice-dependent measure for the amount of focus within an ROI. Thus, selecting the best, i. e. sharpest, slice $z^*_{\mathcal{R}}$ for an ROI $\mathcal{R}$ is a simple maximum operation over all slices z

$$z^*_{\mathcal{R}} = \max_z \left\{ 0.5 \cdot \left(\widehat{\alpha}_{\mathrm{LAPE}}(\mathcal{R}(z)) + \widehat{\alpha}_{\mathrm{LAPD}}(\mathcal{R}(z)) \right) \right\}. \tag{3}$$

Thin-plate spline In order to obtain a smooth and homogeneous image impression, we propose to use a thin-plate smoothing spline (TPS). The TPS fits a mapping function $f(\boldsymbol{x})$ matching the set of coordinate inputs for each ROI $\{\boldsymbol{x}_1 \cdots \boldsymbol{x}_R\}$ with the set of optimal slices $\{z^*_{\mathcal{R}_1} \cdots z^*_{\mathcal{R}_R}\}$, by minimizing the following energy function E

$$E(f(\boldsymbol{x})) = \lambda \cdot \sum_{r=1}^{R} \|z^*_r - f(\bar{\boldsymbol{x}}_r)\|^2 + (1-\lambda) \iint \left[\left(\tfrac{\partial^2 f}{\partial x^2} \right)^2 + 2 \left(\tfrac{\partial^2 f}{\partial x \partial y} \right)^2 + \left(\tfrac{\partial^2 f}{\partial y^2} \right)^2 \right] \mathrm{d}x\, \mathrm{d}y, \tag{4}$$

with $\bar{\boldsymbol{x}}_r$ as central point of the r-th ROI, and λ as smoothing parameter controlling the amount of how much non-ridged transformation is allowed [5].

The determined function f maps each image pixel to a certain slice which is optimal according to the auto-focus measures and the smoothness criterion. Since the resulting value is not necessarily an integer, we apply linear interpolation between the two neighboring slices to obtain the actual projection value.

2.3 Experiment

For proof of concept, we simulated a scan with a female XCAT full-body phantom [6]. In total 380 anterior-posterior noise-free projections (1440x1440 pixel á 0.296 mm with SID = 180 cm and a parallel-shift of 5 mm) were acquired using the presented trajectory and reconstructed using filtered backprojection with $N_z = 100$, a slice thickness $d_z = 3$ mm and an isotropic pixel size $d_x = d_y = 1$ mm.

For evaluation an average intensity projection, i. e. a parallel projection over all slices as well as a conventional full-body radiograph acquired with the Siemens Healthineers SmartOrtho$^{\mathrm{TM}}$-technique was generated.

3 Results

Fig. 3 shows a plot of the auto-focus measures for the right knee, the upper part of the hip, as well as the cervical spine. The dotted red line indicates the expert-annotated ground truth (GT), regarding which slices are optimal w.r.t. sharpness. From this data, we computed the TPS which is presented in Fig. 4. The

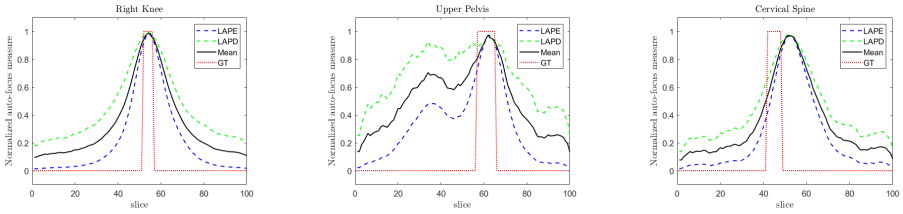

(a) Right knee (b) Upper pelvis (c) Cervical spine

Fig. 3. Auto-focus measures for the right knee (a), the upper pelvis (b) and the cervical spine (c). LAPE is plotted in blue, LAPD in green and the combined mean focus measure in black. The dotted red line indicates the expert-annotated ground truth (GT).

black dots indicate the sampling points, i. e. the central points of the ROIs $\bar{\boldsymbol{x}}$ and the corresponding slice $z^*_{\mathcal{R}}$. For illustration, the 3-D view, as well as the y-z plane, is shown. Fig. 5 shows a comparison of the full-body smart synthetic ra-

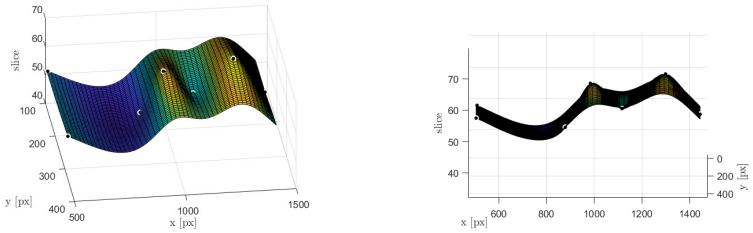

(a) Spline in 3-D (b) Spline in the y-z plane

Fig. 4. Exemplary thin-plate spline in 3-D and the corresponding y-z plane view.

diograph (sSR), an average intensity projection (AIP) as well as a conventional 2-D full-body acquisition (CR). The computation time of the complete algorithm was about 2 seconds.

4 Discussion

We proposed an algorithm which automatically generates a smart synthetic radiograph from a tomosynthetic reconstruction. It was shown that it is possible to

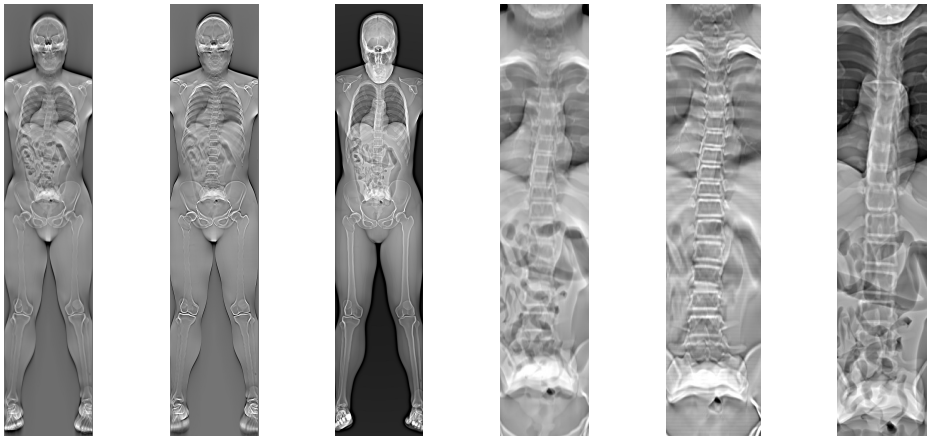

(a) AIP (b) sSR (c) CR (d) AIP (e) sSR (f) CR

Fig. 5. Comparison of an average intesity projection [AIP] (a,d), the smart synthetic radiograph [sSR] (b,e) and a conventional 2-D full-body acquistion [CR] (c,f) for the full body (a,b,c) and a detail view of the spine (d,e,f).

use auto-focus measures to select the slices within a reconstruction which were also considered to be optimal during an expert annotation. Yet, in Fig. 3(c) the method did not work as expected which might be due to low image contrast. The obtained thin-plate spline ensures that predefined ROIs are clearly visible and guarantees an overall homogeneous image impression. Furthermore, the double S-shape of the spine is clearly visible in Fig. 4(b). While on the one hand, the smart radiograph has an overall sharp impression especially of the spine as can be seen in Fig. 5, the standard synthetic radiograph suffers from overlapping structures and the state-of-the-art full-body radiograph approach from overlapping structures and distortion and magnification. As a topic for future research, the selection of the ROIs, which is currently done manually, could be replaced by an automated detection using, for instance, deep neural networks.

References

1. Dobbins JT. Tomosynthesis imaging: at a translational crossroads. Medical physics. 2009;36(6):1956–1967.
2. Lauritsch G, Härer WH. A theoretical framework for filtered backprojection in tomosynthesis. In: Proc. SPIE. vol. 3338; 1998. p. 1127–1137.
3. Luckner C, et al. Parallel-Shift Tomosynthesis for Orthopedic Applications. Proc SPIE. 2018;.
4. Sun Y, Duthaler S, Nelson BJ. Autofocusing in computer microscopy: selecting the optimal focus algorithm. Microscopy research and technique. 2004;65(3):139–149.
5. Bookstein FL. Principal warps: Thin-plate splines and the decomposition of deformations. IEEE Trans Pattern Anal Mach Intell. 1989;11(6):567–585.
6. Segars WP, et al. Realistic CT simulation using the 4D XCAT phantom. Medical physics. 2008;35(8):3800–3808.